J. of Thermal Science Vol.5, No.1

Forced Convective Heat Transfer in a Plate Channel Filled with Solid Particles

Pei-Xue Jiang Ze-Pei Ren Bu-Xuan Wang Zhan Wang

Department of Thermal Engineering, Tsinghua University, Beijing 100084 China

A numerical study of fluid flow and convective heat transfer in a plate channel filled with solid (metallic) particles is presented in this paper. The study uses the thermal equilibrium model and a newly developed numerical model which does not assume idealized local thermal equilibrium between the solid particles and the fluid. The numerical simulation results are compared with the experimental data in reference [2]. The paper investigates the effects of the assumption of local thermal equilibrium versus non–thermal equilibrium, the thermal conductivity of the solid particles and the particle diameter on convective heat transfer.

For the conditions studied, the convective heat transfer and the temperature field assuming local thermal equilibrium are much different from that for the non–thermal equilibrium assumption when the difference between the solid and fluid thermal conductivities is large. The relative values of the thermal conductivities of the solid particles and the fluid also have a profound effect on the temperature distribution in the channel. The pressure drop decreases as the particle diameter increases and the convective heat transfer coefficient may decrease or increase as the particle diameter increases depending on the values of $\varepsilon, \lambda_s, \lambda_f, \lambda_d, \alpha_v, \rho_u$.

Keywords: porous media, local thermal equilibrium; non-thermal equilibrium, particle diameter, convective heat transfer.

INTRODUCTION

Heat transfer enhancement techniques play very important roles in thermal control technologies used for microelectronic chips, powerful laser mirror, aerospace craft, thermal nuclear fusion, etc. Porous structures intensify the mixing of the flowing fluid and enhance the convective heat transfer. Therefore, single-phase flow through porous media is an effective method for cooling structural parts and surfaces receiving a high heat flux. In recent decades, several cooling systems using microchannels or porous structures have been used for mirrors in powerful lasers. Jeigarnik et al.[1,2] and Haritonov et al.[3] numerically and experimentally investigated convective heat transfer on flat plates and in channels filled with porous materials. Their results show that the porous media may increase the heat transfer coefficient 5-10 times although the hydraulic resistance was increased even more. Subbojin and Haritonov[4] gave an overall review of heat transfer and flow characteristics in the cooling systems of powerful lasers using porous matrix materials. They point out that the use of porous media can greatly intensify the heat transfer and very high heat fluxes (4×10^7 W/m^2) can be obtained using single–phase water. As pointed out by Nasr et al.[5], in the on–going search for techniques to augment convective heat transfer, attention has been directed at the possibility of embedding the heat transfer surface in a packed bed.

In recent years, the influence of the non–Darcian effects; variable porosity, variable properties, and thermal dispersion in the porous medium; on the fluid flow and heat transfer have been widely studied, for example, by Choi and Kulacki[6], Kwendakwema and Boehm[7], Wang and Du[8], David et al.[9], Hsu and Cheng[10], Clarksean et al.[11] and Jiang et al.[12,13]. A comprehensive review of heat and fluid flow characteristics in packed beds was published by Achenbach[14].

Received January, 1996.

Notation

c_p	fluid specific heat [J/kgK)]
d_p	particle diameter [m]
F	inertia coefficient [dimensionless]
h	channel height [m]
h_f	fluid specific enthalpy [J/kg]
h_f^+	dimensionless fluid specific enthalpy, $(h_f - h_o)/(q_w c_{po} h/\lambda_{fo})$
K	permeability of porous medium [m^2]
L	channel length [m]
N	number of divisions in x direction
p	pressure [Pa]
p^+	dimensionless pressure, $p/(\rho_o u_o^2)$
Δp	pressure drop [Pa]
Pr	Prandtl number, ν/α, [dimensionless]
q	heat flux [W/m^2]
Re	Reynolds number [dimensionless]
T	temperature [K]
u_p	pore velocity in x direction [m/s]
u_p^+	dimensionless pore velocity in x direction, u_p/u_o
U_p	absolute value of pore velocity, $(u_p^2 + \nu_p^2)^{1/2}$
ν_p	pore velocity in y direction [m/s]
ν_p^+	dimensionless pore velocity in y direction, ν_p/u_o
x, y	coordinates in the flow region [m]
x^+	dimensionless x coordinate, x/h
y^+	dimensionless y coordinate, y/h

Greek symbols

α	heat transfer coefficient [$W/(m^2K)$]
α_x	local heat transfer coefficient [$W/(m^2K)$]
α_e	average heat transfer coefficient [$W/(m^2K)$]
α_v	volumetric heat transfer coefficient between solid particles and fluid [$W/(m^3K)$]
λ	thermal conductivity [W/(mK)]
λ_d	dispersive component of thermal conductivity [W/(mK)]
λ_f	fluid thermal conductivity [W/(mK)]
λ_m	stagnant effective thermal conductivity of fluid and porous media [W/(mK)]
λ_s	solid particles thermal conductivity [W/(mK)]
λ_{ma}	thermal conductivity of solid particle material [W/(mK)]
μ	fluid absolute viscosity [Ns/m^2]
μ_e	effective absolute viscosity [Ns/m^2]
ν	kinematic viscosity [m^2/s]
ρ	fluid density [kg/m^3]
ε	porosity, [dimensionless]
ε_∞	mean porosity, [dimensionless]

Superscripts

$+$	dimensionless quantity
overline	average values

Subscripts

1	upper wall
2	lower wall
b	bulk mean temperature
d	dispersion
f	fluid
p	pore
s	solid
o	heated section inlet
w	wall

But there are yet some problems that need to be investigated further. For example, the model for the additional thermal conductivity resulting from thermal dispersion needs to be perfected. Kwendakwema and Boehm[7], Wang and Du[8], David et al.[9] and Jiang et al.[12,13] found that heat transfer increases as the particle diameter increases, but Jeigarnik et al.[2] and Nasr et al.[5] found the opposite result. Jeigarnik et al.[2] and Nasr et al.[5] related their results to the heat transfer surface increase as the particle diameter decreases. Jiang et al.[13] explained their different conclusions by noting that the experiments of Jeigarnik et al.[2] used water flowing through the packed bed made of metallic particles, and the experiments of Nasr et al.[5] used air flowing through a packed bed of aluminum, alumina, glass and nylon spherical particles. In both cases, the thermal conductivity of the particles (metallic) was much higher than the fluid (water and air), so the heat transfer coefficients on the wall were controlled mainly by conduction heat transfer from the solid particles to the wall. When d_p decreased, the contact surface between the wall and the particles increased, so the heat transfer coefficient increased. In the research of Kwendakwema and Boehm[7], Wang and Du[8], David et al.[9], and Jiang et al.[12,13], the thermal conductivity of the particles (glass) and the fluids (water) were of the same order; therefore, the heat transfer coefficients on the wall were controlled mainly by the convective heat transfer in the bulk fluid. When d_p increased, the thermal dispersion increased and, hence, the heat transfer intensified. The possible non-linear effects of the particle diameter, d_p, on the convective heat transfer coefficient will be analyzed in detail in the present work. A deeper understanding of the effect of the particle diameter on convective heat transfer phenomena in porous media will lead to improved optimization of heat exchangers using porous structures.

Kuo et al.[15], Sozen and Vafai[16] and Florio et al.[17] studied the flow and heat transfer in a cryogenic packed-bed regenerator, the condensing flow of a gas through a packed bed and the thermally-induced response of a decomposing glass-filled polymer composite, assuming non-thermal equilibrium between the solid and fluid phases. Florio et al.[17] predicted deviations from local-thermal equilibrium as high as 200°C. Most previous theoretical analysis and numerical simulations for convective heat transfer of single-phase fluids in porous media assumed local-thermal equilibrium between the solid particles and the fluid. Haritonov et al.[3] pointed out that the temperatures of the fluid and the solid matrix (metallic particles) are not the same, although there is intensive mixing of the fluid in the porous media. This paper compares the thermal equilibrium model and a newly developed numerical model which does not employ the local thermal equilibrium assumption between the solid particles and fluid using a numerical study of fluid flow and convective heat transfer in a plate channel filled with solid (metallic) particles. The numerical simulation results are compared with experimental data in Jeigarnik et al.[2]. The study considers the effect of assuming local thermal equilibrium versus non-thermal equilibrium, the conductivity of the solid particles and the particle diameter on convective heat transfer.

PHYSICAL MODEL AND MATHEMATICAL FORMULATION

The physical model and the coordinate system are shown in Fig.1. The model considers fluid flow and convective heat transfer in a plate channel filled with homogeneous, isotropic solid particles. The upper plate of the channel received a constant heat flux, q_{1w}, while the lower plate was adiabatic. Flow entered the channel with an average velocity, u_o, and constant temperature, T_{fo}. An adiabatic section existed before the heated section. The fluid is single-phase and the flow is two-dimensional, steady, non-Darcian flow. Because only high Peclet number flow is treated, longitudinal conduction in the fluid and the pressure variation in y direction are negligibly small.

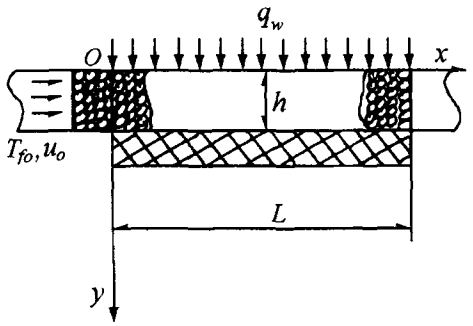

Fig.1 Schematic diagram of the physical system

The steady state, two-dimensional governing equations for single-phase fluid flow in an isotropic, homogeneous porous medium based on Brinkman-Darcy-Forchheimer model with the consideration of variable properties, variable porosity and thermal dispersion can be written in the following form:

$$\frac{\partial(\rho_f \varepsilon u_p)}{\partial x} + \frac{\partial(\rho_f \varepsilon \nu_p)}{\partial y} = 0 \tag{1}$$

$$\frac{\partial(\rho_f \varepsilon u_p u_p)}{\partial x} + \frac{\partial(\rho_f \varepsilon \nu_p u_p)}{\partial y} = -\frac{\partial(\varepsilon p)}{\partial x} - \varepsilon^2 \frac{\mu_f}{K} u_p - \varepsilon^3 \frac{\rho_f F}{\sqrt{K}} |U_p| u_p + \frac{\partial}{\partial y}\left(\varepsilon \mu_e \frac{\partial u_p}{\partial y}\right) \tag{2}$$

$$\int_o^h \rho_f \varepsilon u_p dy = \rho_o u_o h \tag{3}$$

The energy equation for the fluid and solid phases assuming thermal equilibrium, $T_s(x,y) = T_f(x,y)$, can be written as:

$$\frac{\partial(\rho_f \varepsilon u_p h_f)}{\partial x} + \frac{\partial(\rho_f \varepsilon \nu_p h_f)}{\partial y} = \frac{\partial}{\partial y}\left[\frac{(\lambda_m + \lambda_d)}{c_{pf}} \frac{\partial h_f}{\partial y}\right] \tag{4}$$

Using the non-thermal equilibrium model, $T_s(x,y) \neq T_f(x,y)$, the fluid phase and solid phase energy equations are:

$$\frac{\partial(\rho_f \varepsilon u_p h_f)}{\partial x} + \frac{\partial(\rho_f \varepsilon \nu_p h_f)}{\partial y} = \frac{\partial}{\partial y}\left[\frac{(\lambda_f + \lambda_d)}{c_{pf}} \varepsilon \frac{\partial h_f}{\partial y}\right] + \alpha_\nu (T_s - T_f) \tag{5}$$

$$\frac{\partial}{\partial x}\left[\lambda_s (1-\varepsilon) \frac{\partial T_s}{\partial x}\right] + \frac{\partial}{\partial y}\left[\lambda_s (1-\varepsilon) \frac{\partial T_s}{\partial y}\right] - \alpha_\nu (T_s - T_f) = 0 \tag{6}$$

The corresponding boundary conditions are:

$$x = 0,\ u_p = u_p(y),\ \nu_p = \nu_p(y),\ T_f = T_{f0}$$

$$y = 0,\ u_p = \nu_p = 0,$$

$$q_{1w} = q_w = -\lambda_f \partial T_f / \partial y = -\lambda_s \partial T_s / \partial y$$

$$y = h,\ u_p = \nu_p = 0,\ q_{2w} = 0$$

Parameters used in Eqs.1-6 were obtained from Haritonov et al.[3], Jiang et al.[12], Achenbach[14], Cheng et al.[18] and Zehner and Schlunder[19]:

$$K = d_p^2\varepsilon^3/(150(1-\varepsilon)^2);$$

$$F = 1.75/(\sqrt{150}\varepsilon^{3/2});$$

$$\lambda_d = 0.025(\rho c_p)_f d_p|U_p|(1-\varepsilon);$$

$$\varepsilon = \varepsilon_\infty(1 + C_\varepsilon \cdot e^{-2y/d_p}) \quad (0 \le y \le h/2);$$

$$\varepsilon = \varepsilon_\infty\left[1 + C_\varepsilon \cdot e^{-2(h-y)/d_p}\right] \quad (h/2 \le y \le h)$$

$$\frac{\lambda_m}{\lambda_f} = \left[1 - \sqrt{1-\varepsilon}\right] + \frac{2\sqrt{1-\varepsilon}}{1-\sigma B} \times\left[\frac{(1-\sigma)B}{(1-\sigma B)^2}\ln\left(\frac{1}{\sigma B}\right) - \frac{B+1}{2} - \frac{B-1}{1-\sigma B}\right]$$

$$B = 1.25((1-\varepsilon)/\varepsilon)^{10/9};$$

$$\lambda_s = \lambda_{ma}(1-\varepsilon)/(1+\varepsilon);$$

$$\sigma = \lambda_f/\lambda_s$$

$$Nu = \alpha d_p/\lambda_f = \left[(1.18Re^{0.58})^4 + 10.23Re_h^{0.75}\right]^{1/4},$$

(Achenbach's formula)

$$Nu = \alpha d_p/\lambda_f = \left[1 + 1.5(1-\varepsilon)\right](2 + \sqrt{Nu_l^2 + Nu_t^2});$$

(Gnielinski's formula)

$$Nu_l = 0.664Pr^{1/3}(Re/\varepsilon)^{1/2}$$

$$Nu_t = \frac{0.037(Re/\varepsilon)^{0.8}Pr}{1 + 2.443(Re/\varepsilon)^{-0.1}(Pr^{2/3}-1)}$$

$$Re = \varepsilon\rho u_p d_p/\mu;$$

$$Re_h = Re/(1-\varepsilon);$$

$$\alpha_v = \alpha \cdot 6(1-\varepsilon)/d_p$$

In momentum equation, Eq.(2), the terms on the left-hand side are the inertia terms. The terms on the right-hand side are the pressure gradient term, the Darcy term, the Forchheimer term and the Brinkman term, respectively. When $\varepsilon = 1$, K is infinity and the momentum equation describes Newtonian fluid in a parallel plate channel without porous media. Therefore, Eq.(2) is suitable for $0 < \varepsilon \le 1$. The thermophysical properties of water were obtained from Rivkin and Aleksandrov[20] in tabular form. The property values used in the calculations were determined by second-order interpolation relative to enthalpy.

NUMERICAL METHOD

The governing equations for the problem under consideration are coupled and non-linear, making analytical solution impossible. Therefore, the equations were solved numerically using the finite difference method. With the appropriate dimensionless parameters, the governing equations, Eqs. (1)-(6), and the boundary conditions were first transformed into dimensionless form. Then, the dimensionless governing equations were discretized using control volume integration. The fluid phase equations, Eqs.(1)-(5), are parabolic in x. Therefore, when the local-thermal equilibrium model is employed, $T_s(x,y) = T_f(x,y)$, the solution for Eqs.(1)-(4) can march in the downstream direction, Jiang et al.[12,13]. However, when the non-thermal equilibrium model is used, $T_s(x,y) \neq T_f(x,y)$, the solid phase energy equation, Eq.(6), is elliptical and the upstream solid phase temperatures are function of the downstream temperatures. Therefore, iteration is necessary to solve Eq.(6). Since Eqs.(1)-(3),(5) and (6) are coupled to each other, the specific solution procedure was as follows. First, for a particular axial location, the algebraic dimensionless forms of Eqs.(2) and (3) were solved simultaneously for the unknowns u_p^+ and p^+. The velocities, v_p^+, were then evaluated from the continuity equation, Eq.(1). Then the fluid phase energy equation, Eq.(5), was integrated to obtain the fluid enthalpies, h_f^+. Fluid temperatures and thermophysical properties were then evaluated by second-order interpolation. The solid phase energy equation, Eq.(6), was then iterated to obtain the solid phase temperatures, T_s. The algorithm then recalculated u_p^+, p^+, v_p^+, h_f^+ and T_s with the updated physical properties for as many as 20 iterations. The above procedures were then repeated for the next axial location. After the solution transversed the entire length of the channel, the algorithm returned to the initial axial location and the above procedures were then repeated until all of the convergence criteria were satisfied. Due to the no-slip boundary conditions and variable porosity, steep velocity gradients were expected near the wall. Therefore, a non-uniform grid was employed with 202 grid points normal to the wall and 202 grid points in the axial direction.

The desired convective heat transfer parameters were evaluated as follows:
Local heat transfer coefficient on the upper wall:

$$\alpha_x = \frac{q_{1w}}{T_{1w}(x) - T_{fb}(x)} \tag{7}$$

Average heat transfer coefficient on the upper wall:

$$\alpha_e = \frac{q_{1w}}{\overline{T}_{1w}(x) - \overline{T}_{fb}(x)} \tag{8}$$

Pressure drop:

$$\Delta p = \left| \rho_o u_o^2 \sum_{j=2}^{N} \left(\left(\frac{dp^+}{dx^+} \right)_j (\Delta x^+)_j \right) \right| \tag{9}$$

RESULTS AND DISCUSSION

In the numerical calculations, water at T_{fo} = 298.2K was used except where noted. The results were checked in numerous ways to verify the reliability of the physical–mathematical model, the solution procedures and the numerical simulation program. When the heat flux, q_{lw}, was small or the mass flux, $\rho_o u_o$, was very large, the temperature distribution in the fluid and in the solid particles was nearly the same regardless of whether variable thermophysical properties or constant thermophysical properties were used in the calculation. The numerically predicted pressure drop per unit length and average convective heat transfer coefficient on the upper plate surface were compared with values measured experimentally by Jeigarnik et al.[2] in Fig.2 and Fig.3. Discussion of the results in the next section leads to implications for the models currently used to predict pressure drop and heat transfer in porous media. After comparing the numerical and experimental results, the effects of solid phase thermal conductivity and particle diameter are discussed in detail.

Comparison of Numerically Predicted and Experimentally Measured Data:

Measurements by Roblee et al.[21] and Benenati and Brosilow[22] showed that the porosity of a packed-sphere bed increased from a value of 0.36 ~0.4 in the bulk of the bed to 0.8 ~1.0 at the wall. The porosity variation took the form of a damped oscillatory function with the oscillations damped out at about 4 ~5 sphere diameters from the wall. In the experimental research of Jeigarnik et al.[2], the porous structure was formed by sintered bronze particles, where the average porosity is 0.21~0.25 which is smaller than packed-sphere bed. Therefore, the variation of the porosity in sintered porous structures may be different from general packed beds. Several variable porosity models were used in the numerical calculations. It was found that for the conditions $\varepsilon_\infty = 0.21, h = 1.72$ mm, d_p=0.18 mm and $\varepsilon_\infty = 0.23$, $h = 0.86$ mm, d_p=0.18 mm, when the constant, C_ε, in the variable porosity model was taken as $(0.6/\varepsilon_\infty - 1)$, the numerically calculated values of pressure drop agreed well with the experimental data reported in Jeigarnik et al.[2], Fig.2. For the conditions $\varepsilon_\infty = 0.25$, $h = 1.76$ mm, d_p=0.18 mm, when the constant, C_ε, was taken as $(0.98/\varepsilon_\infty - 1)$, the numerically calculated values of pressure drop basically agreed with the experimental data of Jeigarnik et al.[2]. However, when C_ε was taken as $(0.9/\varepsilon_\infty - 1)$, the numerically calculated pressure drop was higher than that measured experimentally. It is well known that the porosity has a profound effect on the flow field and pressure drop. Therefore, the variable porosity model in sintered porous structures needs further investigation. Achenbach[14] found that at $\varepsilon = 0.4$, a 1% error in ε caused a 4% error in the pressure drop. In the present research, it was found that for $\varepsilon = 0.21$, a 10% error in ε caused a 29% error in Δp.

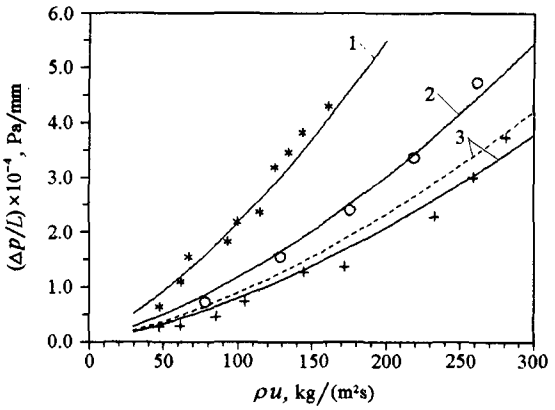

Fig.2 Numerically predicted pressure drop per unit length (*,o,+ – Experimental data[2]; 1,2,3 – Numerically predicted value)
1, * – $h = 1.72$ mm; $\varepsilon_\infty = 0.21$, $C_\varepsilon = 0.6/\varepsilon_\infty - 1$; $d_p = 0.18$ mm
2, o – $h = 0.86$ mm, $\varepsilon_\infty = 0.23$ $C_\varepsilon = 0.6/\varepsilon_\infty - 1$; $d_p = 0.18$ mm
3, + – $h = 1.76$ mm, $\varepsilon_\infty = 0.25$, $C_\varepsilon = 0.98/\varepsilon_\infty - 1$; (solid line) $C_\varepsilon = 0.90/\varepsilon_\infty - 1$ (dotted line): $d_p = 0.18$ mm

As shown in Fig.3 the numerically calculated average convective heat transfer coefficient differed some from the coefficients determined experimentally by Jeigarnik et al.[2], but their overall tendencies are in accordance with each other. The deviations may result from the following: first, the physical model used in the numerical calculation in the present research and the experimental setup used by Jeigarnik et al.[2] were not identical. In the experimental setup, the fluid flowed into and out of the plate porous chan-

nel through small channels placed perpendicular to the heated surface. Secondly, the variable porosity model and the model for the convective heat transfer coefficient between the solid particles and the fluid are not well established. Thirdly, the sintered porous structures may differ significantly from the packed-sphere bed (the well-known physical-mathematical model for convective heat transfer in porous media was developed for the packed-sphere bed). Therefore, the characteristics of sintered porous structures need further study. As shown by curve No.1 in Fig.3, the choice of the local-thermal equilibrium model or the non-thermal equilibrium model between the fluid and solid phases, or the different formulas used to predict the convective heat transfer between the solid particles and the fluid significantly affected the calculated results. Achenbach[14] pointed out that for Reynolds numbers $Re < 500$ the results using Achenbach's formula are lower than those predicted by Gnielinski's formula, as can be seen in Fig.3. The second and third curves in Fig.3 show that the different variable porosity models significantly affect the convective heat transfer, again indicating that more development is needed for the variable porosity model in sintered porous structures.

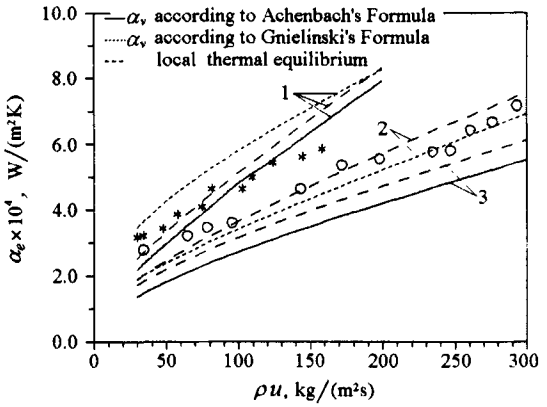

Fig.3 Numerically predicted average heat transfer coefficient (*,o, – Experimental data[2]; 1,2,3 – Numerically predicted value) 1, * – $h = 1.72$ mm; $\varepsilon_\infty = 0.21$, $C_\varepsilon = 0.6/\varepsilon_\infty - 1$; $d_p = 0.18$ mm 2,3, o – $h = 1.76$ mm, $\varepsilon_\infty = 0.25$ $d_p = 0.18$ mm 2, – $C_\varepsilon = 0.90/\varepsilon_\infty - 1$; 3, –$C_\varepsilon = 0.98/\varepsilon_\infty - 1$

Effect of Thermal Conductivity

Fig.4, Fig.5 and Fig.6 show a comparison of analytical solid and fluid temperature profiles for different solid particle thermal conductivities and $\lambda_e = \lambda_f + \lambda_d \approx 12$W/(mK). For the conditions in Fig.4,

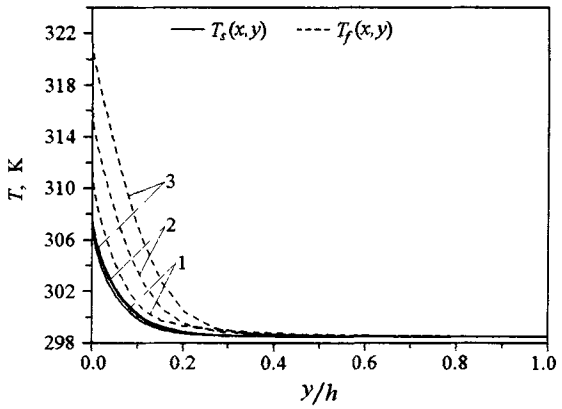

Fig.4 Predicted temperature distribution of solid particles and fluid (λ_{ma}=34 W/(mK)), $\rho_0 u_0 = 160$ kg/(m²s); $q_w = 10^6$ W/m² d_p=0.18 mm; $h = 1.72$ mm; $\varepsilon_\infty = 0.21$; $C_\varepsilon = 0.6/\varepsilon_\infty - 1$; x/h: 1-1.6, 2-3.0, 3-5.2

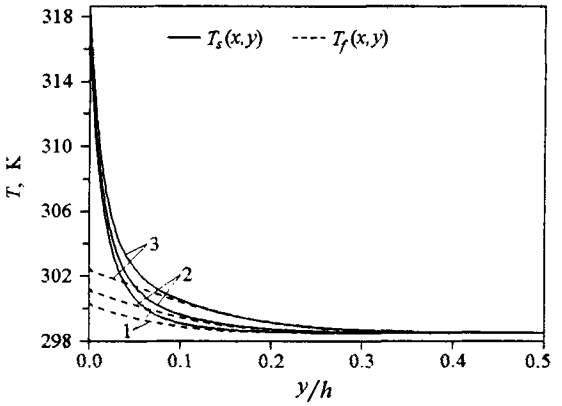

Fig.5 Predicted temperature distribution for solid particles and fluid (λ_{ma}=0.6 W/(mK)), $\rho_0 u_0 = 160$ kg/(m²s); $q_w = 10^5$ W/m² d_p=0,18 mm; $h = 1.72$ mm; $\varepsilon_\infty = 0.21$; $C_\varepsilon = 0.6/\varepsilon_\infty - 1$; x/h: 1-1.6, 2-3.0, 3-5.2

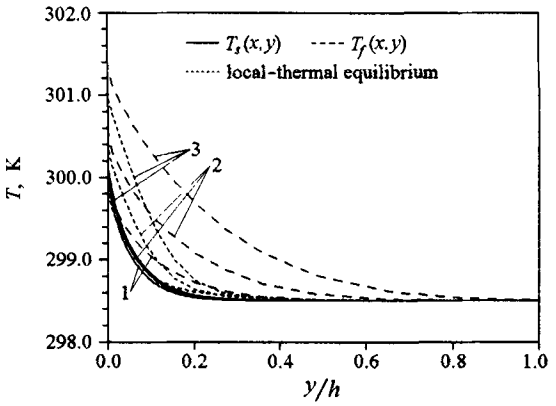

Fig.6 Predicted temperature distribution for solid particles and fluid (λ_{ma}=18.4 W/(mK)), $\rho_0 u_0 = 160$ kg/(m²s); $q_w = 10^5$ W/m² d_p=0.18 mm; $h = 1.72$ mm; $\varepsilon_\infty = 0.21$; $C_\varepsilon = 0.6/\varepsilon_\infty - 1$; x/h: 1-1.6, 2-3.0, 3-5.2

$\lambda_s = 22.2$ W/(mK) and $\lambda_s > \lambda_e$, the temperature of the solid phase near the upper wall was lower than the fluid temperature and the solid–fluid temperature difference increased in the downstream direction and with increasing q_{1w}. Since the porous media can significantly enhance convective heat transfer, the temperature gradient near the upper wall was very large. It can be seen from Fig.4 that when $y > 0.3h$ or $y > 2.9d_p$, the solid particle temperature and the fluid temperature were nearly the same and equal to the inlet temperature, indicating that the heat penetration thickness was $0.3h$ for the given conditions. For the conditions in Fig.5, $\lambda_s = 0.39$ W/(mK)$\ll \lambda_e$, the solid phase temperature near the upper wall was higher than the fluid temperature but for $y > 0.1h$ the solid phase and fluid phase temperatures were equal. It can be found from Fig.6 that when $\lambda_s = 12$ W/(mK)$\approx \lambda_e$, a small difference existed between the solid particle temperature and the fluid temperature using the non–thermal equilibrium model. The temperature profiles predicted using the non–thermal equilibrium model were nearly equal to the temperature predicted using the local–thermal equilibrium model. All temperature profiles were physically reasonable.

Fig.7 shows a comparison of the calculated local convective heat transfer coefficient on the upper wall using the non–thermal equilibrium model and the local–thermal equilibrium model for different solid thermal conductivities. The convective heat transfer coefficient increased as the solid particle thermal conductivity increased. Differences between the non–thermal equilibrium model and the local–thermal equilibrium model disappeared as λ_s approached λ_e. It was found that when the difference between the solid and fluid phase thermal conductivities was not very large, the local–thermal equilibrium model gave satisfactory results for simulating the pressure drop and convective heat transfer, but did not give a correct temperature distribution, especially for very high heat flux. Therefore, to accurately simulate the convective heat transfer process in porous media with large differences in thermal conductivity between solid and fluid phases, the non–thermal equilibrium model needs to be improved, which is the objective of our future experimental and theoretical research.

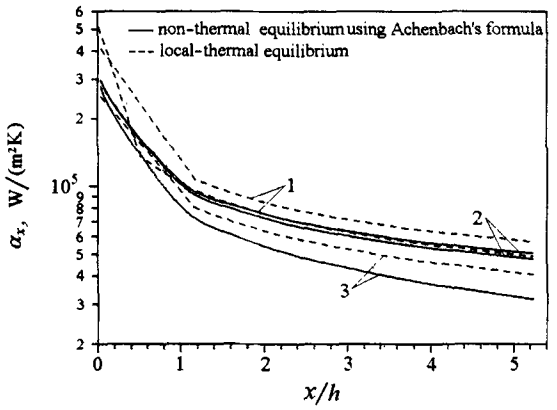

Fig.7 Predicted local heat transfer coefficient
$\rho_0 u_0 = 160$ kg/(m^{2}s); $q_w = 10^5$ W/m^2
d_p=0.18 mm; $h = 1.72$ mm
$\varepsilon_\infty = 0.21$; $C_\varepsilon = 0.6/\varepsilon_\infty - 1$;
λ_{ma} [W/(mK)]: 1-200, 2-34,3-1.

Effect of Solid Particle Diameter

As mentioned earlier, there are some contradictory conclusions concerning the dependence of the convection heat transfer coefficient on the solid particle diameter, d_p, in the works of Jeigarnik et al.[2], Nasr et al.[5], Kwendakwema and Boehm[7], Wang and Du[8], David et al.[9], and Jiang et al.[12,13]. In the following section, the influence of d_p on pressure drop and convective heat transfer coefficient is analyzed in detail theoretically and numerically. Numerical results are presented in Figs.8-15.

In the parameters used in the governing equations, there are 4 parameters – $K, \varepsilon, \lambda_d, \alpha_\nu$, that are direct functions of d_p. The expressions for K and ε show that K and ε increase near the wall as d_p increases, so the pressure drop should decrease based on physical reasoning. The numerical simulation results, Fig.8, assuming either constant porosity or variable porosity show that the pressure drop does indeed decrease as d_p increases.

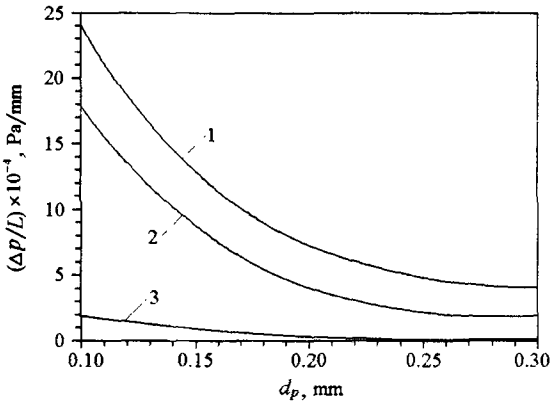

Fig.8 Effect of particle diameter on pressure drop per unit length
$h = 1.72$ mm, $\varepsilon_\infty = 0.21$,
$C_\varepsilon = 0.6/\varepsilon - 1$; $q_w = 10^5$ W/m^2;
1–ε =constant, $\rho_0 u_0 = 200$ kg/(m^{2}s);
2–ε =variable, $\rho_0 u_0 = 200$ kg/(m^{2}s);
3–ε =variable, $\rho_0 u_0 = 30$ kg/(m^{2}s).

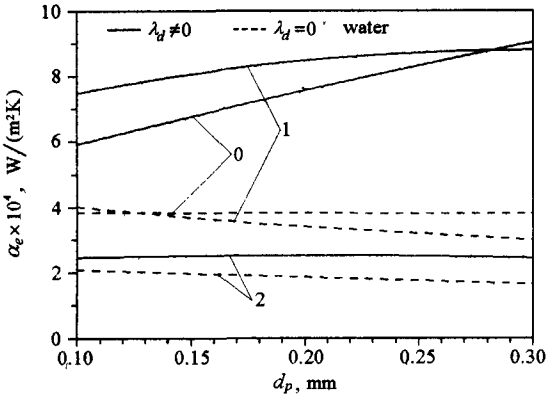

Fig.9 Effect of particle diameter on average heat transfer coefficient (λ_{ma} = 34 W/(mK)); h = 1.72 mm, ε = 0.21, $C_\varepsilon = 0.6/\varepsilon_\infty - 1$
0–ε =constant, $\rho_0 u_0$ = 200 kg/(m²s);
1–ε =variable, $\rho_0 u_0$ = 200 kg/(m²s);
2–ε =variable, $\rho_0 u_0$ = 30 kg/(m²s);
$q_w = 10^5$ W/m².

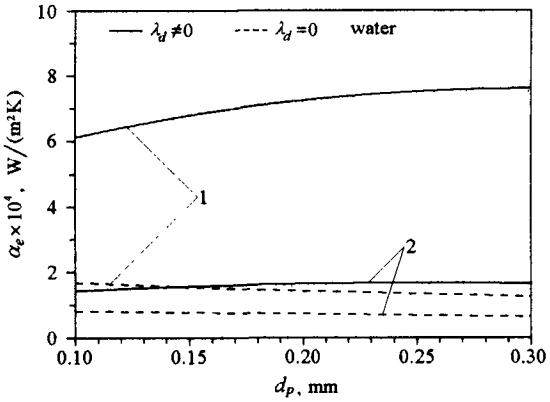

Fig.10 Effect of particle diameter on average heat transfer coefficient (λ_{ma} = 1 W/(mK)); h = 1.72 mm, ε_∞ = 0.21, $C_\varepsilon = 0.6/\varepsilon_\infty - 1$
$q_w = 10^5$ W/m²;$\rho_0 u_0$ [kg/(m²s)]:1-200;2-30.

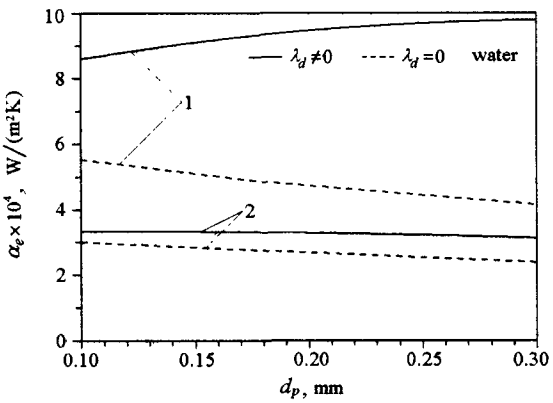

Fig.11 Effect of particle diameter on average heat transfer coefficient (λ_{ma} = 200 W/(mK)); h = 1.72 mm, ε_∞ = 0.21, $C_\varepsilon = 0.6/\varepsilon_\infty - 1$
$q_w = 10^5$ W/m²;$\rho_0 u_0$ [kg/(m²s)]:1-200;2-30.

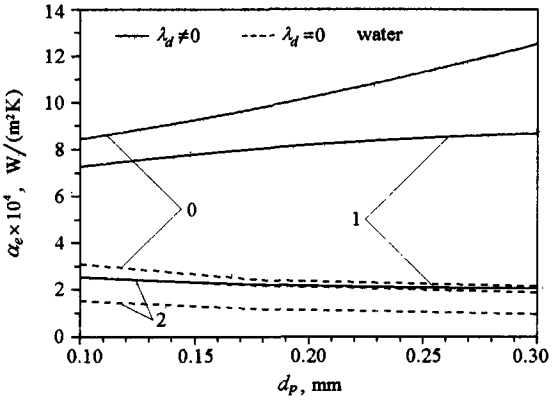

Fig.12 Effect of particle diameter on average heat transfer coefficient (λ_{ma} = 34 W/(mK)); h = 2 mm, ε_∞ = 0.21, $C_\varepsilon = 0.6/\varepsilon_\infty - 1$
0–ε=constant; $\rho_0 u_0$=200 kg/(m²s)
1–ε=variable, $\rho_0 u_0$=200 kg/(m²s)
2–ε=variable, $\rho_0 u_0$=30 kg/(m²s)
$q_w = 10^5$ W/m²

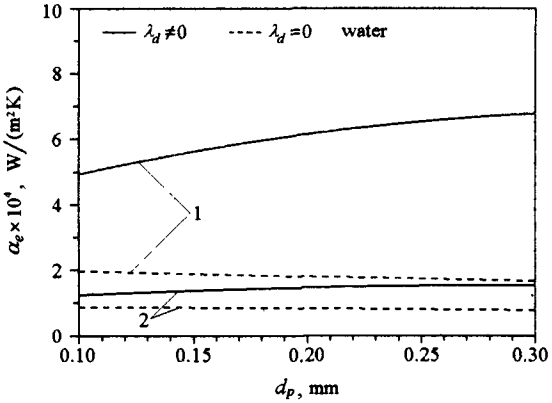

Fig.13 Effect of particle diameter on average heat transfer coefficient (λ_{ma} = 1 W/(mK)); h = 2 mm, ε_∞ = 0.21, $C_\varepsilon = 0.6/\varepsilon_\infty - 1$
$q_w = 10^5$ W/m²;$\rho_0 u_0$ [kg/(m²s)]:1-200;2-30.

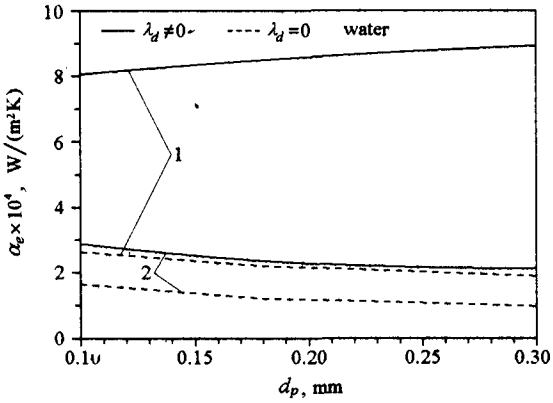

Fig.14 Effect of particle diameter on average heat transfer coefficient (λ_{ma} = 200 W/(mK)); h = 2 mm, ε_∞ = 0.21, $C_\varepsilon = 0.6/\varepsilon_\infty - 1$
$q_w = 10^5$ W/m²;$\rho_0 u_0$ [kg/(m²s)]:1-200;2-30.

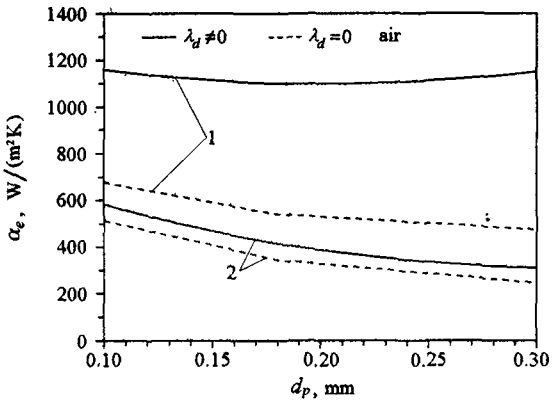

Fig.15 Effect of particle diameter on average heat transfer coefficient (λ_{ma} = 1.01 W/(mK)); h = 2 mm, ε_∞ = 0.21, $C_\varepsilon = 0.6/\varepsilon_\infty - 1$ $q_w = 10^4$ W/m²;$\rho_0 u_0$ [kg/(m²s)]:1-10;2-1.0;

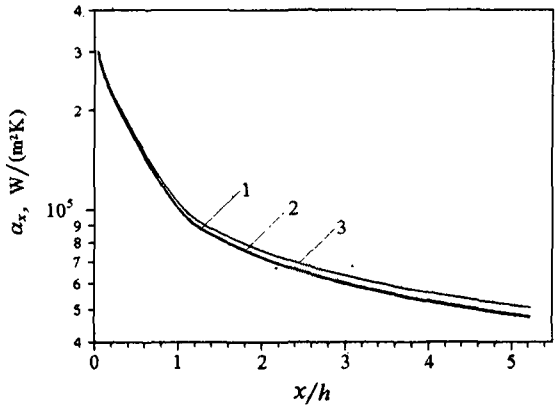

Fig.16 Predicted local heat transfer coefficient for different heat fluxes (λ_{ma} = 34 W/(mK)); $\rho_0 u_0$ = 160 kg/(m²s); d_p = 0.18 mm; h = 1.72 mm, ε_∞ = 0.21; $C_\varepsilon = 0.6/\varepsilon_\infty - 1$ q_w [w/m²]: 1-10³; 2-10⁵; 3-10⁶)

A simplified theoretical analysis assumes that local-thermal equilibrium exists between the solid matrix and the fluid. Consideration of the energy equation, Eq.(4), suggests that when the additional thermal conductivity resulting from thermal dispersion, λ_d, is not considered and the porosity is assumed to be constant, the effect of d_p on convective heat transfer may be not great, as confirmed by the No.0 dotted line in Fig.9. Using variable porosity, the porosity near the wall increases as d_p increases which weakens the mixing of the fluid by the porous media. Therefore, as shown by No.1 and No.2 dotted lines in Figs.9-11, the convective heat transfer coefficient on the upper wall decreases. When considering only thermal dispersion effect, the formula for λ_d shows that λ_d increases as d_p increases and the convective heat transfer should be intensified. The circumstance is indeed so for $\varepsilon = const$ as shown by No.1 solid line in Fig.9. But for $\varepsilon \neq const$, the convective heat transfer enhancement due to the increase of λ_d resulting from the increase in d_p may not be enough to counterbalance the decrease in the convective heat transfer due to the increase of ε near the wall as d_p increases. The overall effect depends on the relative values of λ_d and λ_m. Qualitatively, when λ_d is larger than λ_m (when ρu is large or λ_s is small), the convective heat transfer will increase as d_p increases as shown by No.1 solid lines in Figs.9-11 and No.2 solid lines shown in Fig.10. On the other hand, when λ_d is much less than λ_m (when ρu is small or λ_s is very large), the convective heat transfer will decrease as d_p increases, the No.2 solid lines in Fig.9 and Fig.11. The above analysis can be verified by the following quantitative calculation: for ε_∞ = 0.21, and λ_{ma} = 200 W/(mK), 34 W/(mK), 1W/(mK), then λ_m = 14.6 W/(mK), 7.0 W/(mK) and 0.64 W/(mK), respectively. When ρu = 200 kg/m²s and d_p=0.1 mm, 0.18 mm, 0.3 mm, then λ_d = 7.86 W/(mK), 14.2 W/(mK) and 23.6 W/(mK), respectively, i.e. $\lambda_d \geq \lambda_m$. Therefore, α increases as d_p increases as shown by No.1 solid lines in Figs.9-11. When ρu = 30 kg/m²s and d_p=0.1 mm, 0.18 mm, 0.3 mm, then λ_d = 1.18 W/(mK), 2.1 W/(mK) and 3.5 W/(mK), respectively. When $\lambda_d < \lambda_m$, α decreases as d_p increases as shown by No.2 solid lines in Fig.9 and Fig.11. When $\lambda_d > \lambda_m$, α increases as d_p increases as shown by No.2 solid line in Fig.10. These analytical conclusions can be used to qualitatively explain the different results obtained by various researchers: in Jeigarnik et al.[2], the porous matrix material was bronze spheres with water as the working fluid and in Nasr et al.[5], the porous matrix materials were aluminum, alumina, glass, and nylon with air as the working fluid, i.e. $\lambda_m \gg \lambda_f$. When ρu is not very large, λ_d is less than λ_m. Therefore, α decreases as d_p increases. In Kwendakwema and Boehm[7], Wang and Du[8], David et al.[9], and Jiang et al.[12,13]; the solid matrix was glass particles with water as the working fluid, i.e. $\lambda_m \approx \lambda_f$. λ_d is then much larger than λ_m and α increases as d_p increases.

Summarizing the above analysis, the parameter λ_d/λ_m may be used to specify the heat transfer regime: when $\lambda_d/\lambda_m > C, \alpha$ increases as d_p increases and α decreases as d_p decreases. C may be of the order of 1. The criterion can be written as:

$$\rho_0 u_0 d_p > 40 \cdot C \cdot \varepsilon/(1-\varepsilon) \cdot \lambda_m / C_{pf} \qquad (10)$$

When the non-thermal equilibrium assumption between solid and fluid phases is used, the same qualitative conclusion is also obtained, that is: as d_p increases, ε increases near the wall, α_ν decreases and the convective heat transfer decreases. However, the

increase of d_p also enlarges λ_d which tends to enhance convective heat transfer. The final effect of d_p on α depends on the relative values of $\varepsilon, \lambda_s, \lambda_f, \lambda_d, \alpha_\nu, \rho u$, etc. Figs.12-15 show numerically calculated results describing the influence of d_p on α assuming non–thermal equilibrium. It can be seen from Figs.9-15 that for the non–thermal equilibrium assumption, the decrease of α as d_p increases under corresponding conditions is more evident than for the local–thermal equilibrium assumption.

Fig.16 show the influence of variable properties on convective heat transfer. When the heat flux, q_{1w}, is very high, the temperature difference between the wall and the fluid is large enough to cause significant variation of the thermophysical properties which affects the convective heat transfer. It can be seen from Fig.16 that the convective heat transfer coefficient increases as the heat flux increases.

CONCLUSION

For horizontal flow in a plate channel filled with porous medium, the numerical results and comparison with the limited available experimental data suggest the following conclusions:

(1) For the conditions studied, the difference in the convective heat transfer predicted using local thermal equilibrium assumption versus the non–thermal equilibrium assumption is significant when the difference between the solid and fluid thermal conductivities is large. The local thermal equilibrium model can not give a correct temperature field, especially when the heat flux is very high.

(2) The relative values of the thermal conductivity of the solid particles and the fluid have profound effect on the temperature distribution in the channel, especially near the heated wall.

(3) The pressure drop decreases and the convective heat transfer coefficient can decrease or increase as the particle diameter increases depending on the values of $\varepsilon, \lambda_s, \lambda_f, \lambda_d, \alpha_\nu, \rho u$.

(4) When the heat flux, q_{lw}, is very high, variable thermophysical properties influence the convective heat transfer. For the conditions studied, the higher the heat flux, the larger the convective heat transfer coefficient.

Acknowledgments

The project was financially supported by funds from the National Science Foundation of China, National Natural Education Committee Fund for Excellent Young Teachers and the Natural Science Fundamental Research Foundation of Tsinghua University, Beijing, China.

REFERENCES

[1] U.A. Jeigarnik, V.K. Shikov and A.I. Shgipeliman, "Flow in Channel with Bend Filled with Porous Medium," (in Russian), *Teplofizika Vys. Temp.*, **24**, No.5, pp.941-947, (1986).

[2] U.A. Jeigarnik, F.P. Ivanov and N.P. Ikranikov, "Experimental Data on Heat Transfer and Hydraulic Resistance in Unregulated Porous Structures," (in Russian), Teploenergetika, No.2, pp.33-38, (1991).

[3] V.V. Haritonov, U.N. Kiceleva, V.V. Atamanov, U.A. Jeigarnik and F.P. Ivanov, "Generalization of the Results on Heat Transfer Intensification in Channels with Porous Insertion," (in Russian), *Teplofizika Vys. Temp.*, **32**, No.3, pp.433-440, (1994).

[4] V.I. Subbojin and V.V. Haritonov, "Thermophysics of Cooled Laser Mirror," (in Russian), *Teplofizika Vys. Temp.*, **29**, No.2, pp.365-375, (1991).

[5] K. Nasr, S. Ramadhyani and R. Viskanta, "An Experimental Investigation on Forced Convection Heat Transfer from a Cylinder Embedded in a Packed Bed," *J. of Heat Transfer*, **116**, pp.73-80, (1994).

[6] C.Y. Choi and F.A. Kulacki, "Non–Darcian Effects on Mixed Convection in a Vertical Porous Annulus," Proc. 9th IHTC-Heat transfer, **5**, pp.271-276, (1990).

[7] N.J. Kwendakwema and R.F. Boehm, "Parametric Study of Mixed Convection in a Porous Medium between Vertical Concentric Cylinders," *J. of Heat Transfer*, **113**, pp.128-134, (1991).

[8] B.X. Wang and J.H. Du, "Forced Convective Heat Transfer in a Vertical Annuli Filled with Porous Media," *Int. J. Heat Mass Transfer*, **36**, pp.4207-4214, (1993).

[9] E. David, G. Lauriat and P. Cheng, "A Numerical Solution of Variable Porosity Effects on Natural Convection in a Packed–Sphere Cavity," *J. of Heat Transfer*, **113**, pp.391-399, (1991).

[10] C.T. Hsu and P. Cheng, "Thermal Dispersion in a Porous Medium," *Int. J. Heat Mass Transfer*, **33**, No.8, pp.1587-1597, (1990).

[11] R. Clarksean, R. Golightly and R.F. Boehm, "An Experimental and Numerical Investigation of Mixed Convection in a Porous Medium between Vertical Concentric Cylinders," Proc. 9th IHTC-Heat Transfer 1990, Hemisphere, New York, **2**, pp.477-482, (1990).

[12] P.X. Jiang, B.X. Wang and Z.P. Ren, "A Numerical Investigation of Mixed Convection in a Vertical Porous Annulus," 10th Int. Heat Transfer Conference, Brighton, UK, **5**, pp.303-308, (1994).

[13] P.X. Jiang, B.X. Wang, D.A. Luo and Z.P. Ren, "Fluid Flow and Convective Heat Transfer in a Vertical Porous Annulus," accepted by Numerical Heat Transfer, (1996).

[14] E. Achenbach, "Heat and Flow Characteristics of Packed Beds," Experimental Thermal and Fluid Science, **10**, pp.17-27, (1995).

[15] S.M. Kuo, P.E. Phelan and C.L. Tien, "Non–Darcian Analysis of Cryogenic Packed–Bed Regenerators," in : Compact Heat Exchangers, R. K. Shah et al., eds., pp.627-644, (1990).

[16] M. Sozen and K. Vafai, "Analysis of the Non–Thermal Equilibrium Condensing Flow of a Gas Through a Packed Bed," *Int. J. Heat Mass Transfer,* **33,** No.6, pp.1247-1261, (1990).

[17] J. Jr. Florio, J.B. Henderson, F.L. Test and R. Hariharan, "A study of the Effects of the Assumption of Local–Thermal Equilibrium on the Overall Thermally–induced Response of a Decomposing, Glass-filled Polymer Composite," *Int. J. Heat Mass Transfer,* **34,** No.1, pp.135–147, (1991).

[18] P. Cheng, C.T. Hsu and A. Chowdhury, "Forced Convection in the Entrance Region of a Packed Channel with Asymmetric Heating," *J. of Heat Transfer,* **110,** pp.946–954, (1988).

[19] P. Zehner and E.U. Schlunder, "Thermal Conductivity of Granular Materials at Moderate Temperature," (in German), Chemie Ingenieur Technik, **42,** pp.933–941, (1970).

[20] S.L. Rivkin and A.A. Aleksandrov, "Thermophysical Properties of Water and Steam," (in Russian), Moscow Energy Press, (1980).

[21] L.H.S. Roblee, R.M. Baird and J.W. Tiern, "Radial Porosity Variations in Packed Beds," A.I.Ch.E. JI4, pp.460-464, (1958).

[22] R.F. Benenati and C.B. Brosilow, "Void Fraction Distribution in Beds of Sphere," A.I.Ch.E. JI8, pp.359-361, (1962).